Progress In Electromagnetics Research, Vol. 130, 169–186, 2012

INVESTIGATION ON DOPPLER SPECTRAL CHARACTERISTICS OF ELECTROMAGNETIC BACKSCATTERED ECHOES FROM DYNAMIC NONLINEAR SURFACES OF FINITE-DEPTH SEA

D. Nie[1], M. Zhang[1, *], X.-P. Geng[2], and P. Zhou[2]

[1]School of Science, Xidian University, Xi'an 710071, China

[2]Science and Technology on Electromagnetic Scattering Laboratory, Beijing 100854, China

Abstract—The Doppler spectral characteristics of electromagnetic backscattered echoes from dynamic nonlinear surfaces of finite-depth sea is investigated with the second-order small-slope approximation (SSA-II). The revised nonlinear hydrodynamic choppy wave model (CWM) combining with an experiment-verified shoaling coefficient is utilized to model the finite-depth sea wave profiles, and the simulated surfaces of finite-depth sea show steeper crests and more flat troughs as depth decreases. First, Comparison of the Doppler spectra for linear sea surfaces and nonlinear choppy sea surfaces shows that nonlinear hydrodynamic effect greatly enhances the Doppler shift and the Doppler spectrum bandwidth, and the predicted results agree well with the rigorous numerical model data. The Doppler spectra of backscattered echoes from finite-depth sea with different depths are further evaluated. At small incident angles, the Doppler shifts and the spectra bandwidths are much lower for shallower sea, and the opposite situation can be gradually observed for increased incident angles. This indicates that the nonlinear wave-wave interactions among waves occur more frequently in finite-depth sea and the long waves will be suppressed while shorter wind waves will be boosted in shallower water. Moreover, the dependence of the Doppler spectral characteristics on polarization is also discussed.

1. INTRODUCTION

The Doppler spectrum of backscattered echoes provides much more valuable information than the mere radar backscattering cross

Received 25 June 2012, Accepted 4 August 2012, Scheduled 10 August 2012

* Corresponding author: Min Zhang (mzhang@mail.xidian.edu.cn).

section, thus the study of the Doppler spectral characteristics from dynamic oceanic surfaces has been receiving great attention for its myriad applications in research areas such as target detection [1–7], remote sensing in marine environment, etc. [8–10]. With the development of calculation methods, both the asymptotic methods and numerical techniques are resorted to calculate the Doppler spectra and successively explain the experimental observations. Among them, the classical approaches such as the Kirchhoff Approximation (KA) and two-scale model (TSM) are employed to predict the Doppler shifts of backscattered fields from sea surfaces for the case of high-grazing angles and moderate-grazing angles [11, 12]. Unfortunately, beyond their applicable range of angles, as low-grazing angles (LGA), their predictions are inaccurate to some extent. Rino et al. [13] comparatively studied the backscattering and the Doppler spectra from one-dimensional (1-D) time-varying linear and nonlinear Creamer sea surfaces [14] for the first time. Toporkov and Brown [15] made a comprehensive study of the Creamer nonlinear surface scattering characteristics using the method of ordered multiple interactions (MOMI). Their results explicitly showed the higher Doppler shift and broadening of the Doppler spectra for nonlinear sea surfaces. Also applying the MOMI, Johnson et al. [16] carried out a comparative research for different nonlinear sea surface models. Recently, Soriano et al. [17] extended the Doppler spectral analysis to the two-dimensional (2-D) nonlinear surfaces on the basis of small-slope integral equation method. Nouguier et al. [18] combined the so-called nonlinear "choppy wave model" (CWM) [19] with the weighted curvature approximation (WCA) probing the impact of nonlinear wave profiles on scattering from sea surfaces. Compared with other nonlinear surface models, the CWM has been proven to enjoy some desirable properties such as analytical simplicity and numerical efficiency. It is found that the nonlinear hydrodynamics plays an important role in the interpretation of the Doppler spectral characteristics from the sea surfaces.

Most of above studies are limited to infinite-depth sea, however. What will happen if the similar study of Doppler spectral characteristics is carried out in the case of finite-depth sea? This is the motivation of this paper. As nearshore sea of finite depth is a marine range where human activities happen most frequently, the corresponding studies have become significant issues of both the national defense and related civil engineering research. Barrick and Lipa [20, 21] presented details of the analytical techniques for the modeling and inversion of second-order high frequency radar Doppler spectra of sea-echo, they stressed that the hydrodynamic contribution is more important when sea waves move into shallow water. Holden

and Wyatt [22] discussed modifications necessary to account for the effects of shallow water in the simulation and inversion of radar Doppler spectra. In general, as a wave propagates from an infinite-depth sea to a finite-depth region, water depth decreases and the wave slows down, although its frequency remains the same. As a result, it changes shape: its crest becomes shorter and steepens, while its trough lengthens and flattens out. Thus the nonlinear CWM is much appropriate for constructing this kind of surface profiles. In this study, we revised the CWM to take the finite-depth effect into account. Moreover, we just consider sea surfaces of constantly finite depth, the extra effects of wave energy dissipation such as breaking [23, 24] are certainly not taken into account.

Recently, the second-order small-slope approximation (SSA-II) has been widely applied to evaluate electromagnetic (EM) scattering from sea surfaces with great accuracy [25–28]. Compared with rigorous numerical methods such as MOMI based on the iteratively solving the magnetic field integral equation with heavy burden on computation time, the analytical model SSA-II is efficient with acceptable accuracy, thus the SSA-II is employed in this study. In this paper, our goal is to firstly validate the model for Doppler spectral analysis for common infinite-depth sea surface, and on this basis, to carry out study of corresponding Doppler spectral characteristics from finite-depth sea. As aforementioned, Toporkov and Brown provided a set of extensive Doppler simulations based on rigorous EM model for 1-D sea surfaces, to facilitate comparison with their reference work, the numerical calculation and subsequent investigations will thus performed for 1-D sea surfaces in this paper.

The paper is organized as follows. In Section 2, the revised CWM taking the finite-depth effect into account is used to describe surfaces of finite-depth dynamic sea, and corresponding analysis of statistical properties is also provided. Section 3 presents the SSA-II model for evaluating the Doppler spectral characteristics from sea surfaces in detail. Comparison of numerical results of the Doppler spectra for infinite-depth sea and finite-depth sea is presented and discussed in Section 4. Section 5 devotes to the conclusions of the paper.

2. DYNAMIC NONLINEAR MODEL FOR FINITE-DEPTH SEAS

2.1. Sea Spectrum for Finite-depth Sea Water

When the waves propagate into shallow sea region, however, it is essential that the water depth and seabed topography will change the shape and the statistical characteristics of the sea surface.

McCormick [29] studied the depth effects on the wave height based on the assumption that the energy flux is conserved as a wave passes from one water depth to another, and associated this effect with sea spectrum by a so-called shoaling coefficient $\eta(d)$, which is the function of sea depth d and the wave number of the sea wave k. The sea wave frequency f and k can be related according to the shallow-water gravity-capillarity dispersion relation as

$$f = \sqrt{gk\left(1 + k^2/k_m^2\right)\tanh\left(kd\right)}/2\pi \tag{1}$$

where $k_m = 363.2\,\mathrm{rad/m}$ is the wavenumber with minimum phase speed. g is the acceleration of gravity. Thus the sea spectrum for finite-depth sea can be written as

$$S_{\mathrm{finite}}\left(f\right) = S_J\left(f\right)\eta\left(d\right) \tag{2}$$

where $S_J\left(f\right)$ denotes the JONSWAP spectrum [30],

$$S_J\left(f\right) = \frac{\alpha g^2}{\left(2\pi\right)^4 f^5}\exp\left[-1.25\left(\frac{f_m}{f}\right)^4\right]\gamma^{\exp\left[\frac{-(f-f_m)^2}{2\sigma^2 f_m^2}\right]} \tag{3}$$

$\alpha = 0.076(gX/u_{10})^{-0.22}$ is the dimensionless constant that related to the wind fetch X and wind speed u_{10} at 10 m above the mean sea level, and $f_m = 3.5g^{0.67}/(X^{0.33}u_{10}^{0.34})$ is the frequency of the spectral peak. The peak shape parameter $\sigma = 0.07$ (when $f \le f_m$), and $\sigma = 0.09$ (when $f > f_m$). γ is the peak enhancement factor, here we chose its mean value of 3.3 based on measurements in [30].

Figure 1 presents the variation of shoaling coefficient $\eta(d)$ with relative sea depth d/λ_w. λ_w denotes the wavelength of sea wave. It can be seen that the shoaling coefficient in the deep sea area almost

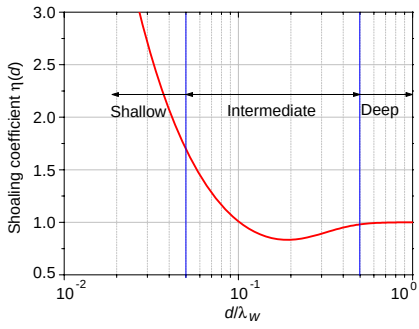

Figure 1. Variation of shoaling coefficient versus relative water depths.

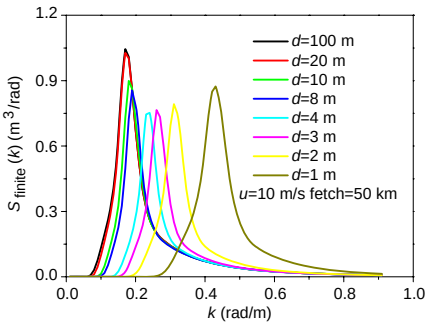

Figure 2. The finite-depth sea spectrum for different water depths.

has a constant value of one; in the intermediate depth area, shoaling coefficient first decreases to the minimum and then increases as the depth reduces; finally, in the shallow sea area, shoaling coefficient rises rapidly. Figure 2 illustrates the finite-depth sea spectrum combining JONSWAP spectrum and shoaling coefficient for different sea depths d. First, when the water depth decreases, the peak values of the curves change following a similar rule to the shoaling coefficient. Second, the peaks of the spectra shift toward the high frequency part as the water depth decreases, which can be explained by the fact that shallower water can sustain only lower and shorter wind waves.

2.2. Sea-surface Realizations

For the fully-developed infinite-depth sea, the spectral method is applied to yield a linear superposition of harmonic waves of whose amplitudes are independent normal-distributed random values times the square root of the sea surface spatial spectrum. This is most efficiently accomplished directly in the Fourier domain. The Fourier amplitudes of a sea surface elevation at time t can be expressed as

$$A(k,t) = \xi(k)\sqrt{S(k)\,\delta k}\exp(j\omega t) + \xi(-k)^*\sqrt{S(k)\,\delta k}\exp(-j\omega t) \quad (4)$$

where $S(k)$ is the sea spectrum, and $\xi(k)$ is a complex Gaussian series with zero mean and unity standard deviation, as well as no correlation between disjoint wavenumbers. The superscript * denotes the conjugation operation. The sampling interval $\delta k = 2\pi/L$, and L is the length of the sea surface along x-axis direction. Based on the gravity-capillarity dispersion relation in Equation (1), angular frequency $\omega = 2\pi f$ can be obtained. Thus the sea surface elevation h at time t can be expressed as

$$h(x,t) = \sum_k A(k,t)\exp(jkx) \quad (5)$$

Equation (5) can be efficiently accomplished by inverse fast Fourier transform (IFFT), and the Hermitian form of Equation (4) ensures that $h(x,t)$ is real.

The nonlinear hydrodynamic model CWM is based on a Lagrangian description of sea wave motion and can be constituted by horizontal displacement of Hilbert transform of an aforementioned linear surface. The displacement is written as

$$C(x,t) = \sum_k -j\frac{k}{|k|}A(k,t)\exp(jkx) \quad (6)$$

Inspired by the Gerstner-Miche model for shallow water description [31], we can rewrite Equation (6) after taking the finite-depth

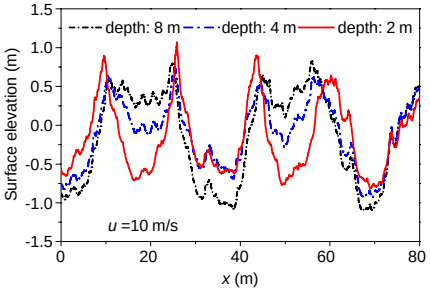

Figure 3. 1-D sea-surface profiles for different d.

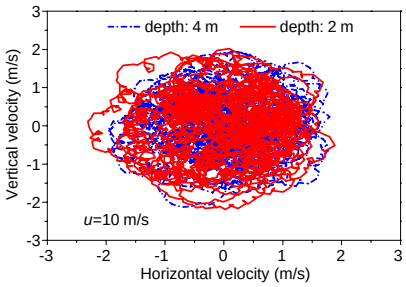

Figure 4. Orbit velocity of surface particles.

effect into consideration

$$C(x,t) = \sum_{k} -j \frac{k}{|k|} \frac{\cosh(kd)}{\sinh(kd)} A(k,t) \exp(jkx) \tag{7}$$

When the water depth d tends to infinite, Equation (7) reduces to Equation (6). Using this function, the horizontal position of a point of the sea surface is now $\tilde{x} = x + C(x,t)$, with elevation $\tilde{h}(\tilde{x},t) = h(x,t)$ as before. This relation can be expressed as

$$\{x, h(x,t)\} \mapsto \{x + C(x,t), h(x,t)\} \tag{8}$$

To clearly show the influences of finite-depth factor on the geometric appearance of the surface, Figure 3 depicts the 1-D sea-surface profiles for different water depths. The wind speed is 10 m/s. As the water depth decreases, the wave crests steepen while wave troughs become much gentler. This property of the nonlinear hydrodynamic finite-depth wave model is more consistent with the actual shallow sea waves. In Figure 4, the horizontal and vertical orbit velocity of the CWM surfaces of finite-depth sea is illustrated. It is clearly shown that the magnitude of the horizontal orbit velocity and the vertical orbit velocity are almost equal. This implies that the horizontal velocity component of the dynamic surface should be considered with great accuracy. This phenomenon also reiterates the importance of the nonlinear hydrodynamics in the process of simulating Doppler spectra of dynamic sea surfaces.

Figure 5 displays the vertical slope of the simulated sea surface with different depths as it evolves in time. The wind speed is 10 m/s and the length of the surface 75 m. To clearly show the magnitude of the slope, we take the absolute value of the surface slope in these plots. The color scales in the four plots are the same from 0.005 to 0.6, and slopes beyond 0.6 are denoted with red color, while slopes below

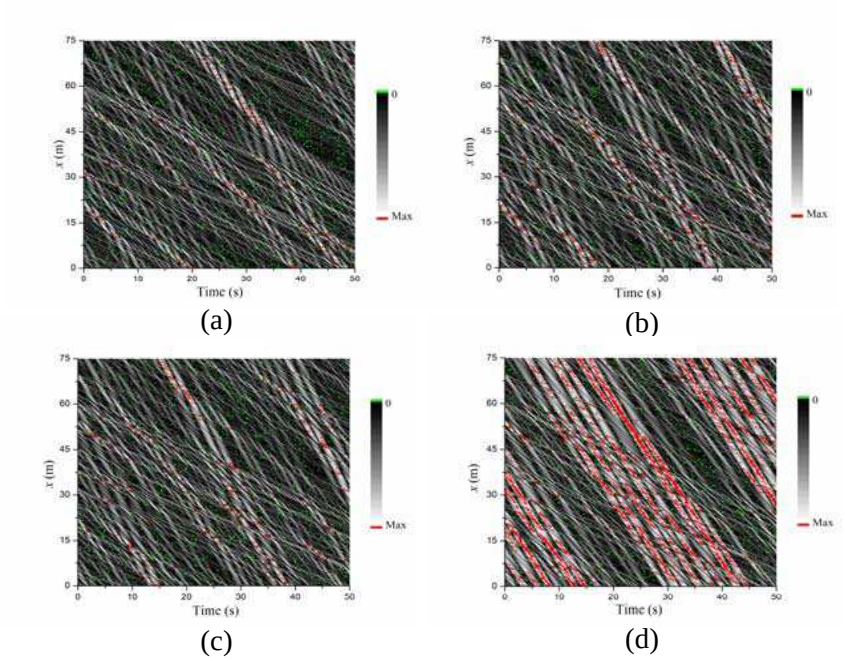

Figure 5. The absolute value of the vertical slope of the simulated sea surface with different depth as it evolves in time. The wind speed u is 10 m/s. (a) Depth: 8 m. (b) Depth: 4 m. (c) Depth: 2 m. (d) Depth: 1 m.

0.005 denoted with green color. It is explicitly shown that the number of points with the large slope of the sea surface becomes bigger and bigger when the water depth decreases. Moreover, as time evolves, corresponding wave crests and troughs propagate steadily with some regularity. From Figure 3 and Figure 5, it can be concluded that the nonlinear hydrodynamic contribution is more important in the finite depth sea.

3. SSA-II MODEL FOR CALCULATION OF THE DOPPLER SPECTRUM

In this section, the SSA-II is applied to calculate the Doppler spectrum. Consider a tapered plane wave illuminating upon a 1-D sea surface to eliminate the edge effect caused by choosing limited size surface. The geometry of the scattering problem is illustrated in Figure 6. θ_i and θ_s denote the incident angle and scattered angle. The incident wave vector $\mathbf{k}_i$ and scattering wave vector $\mathbf{k}_s$ can be decomposed into their

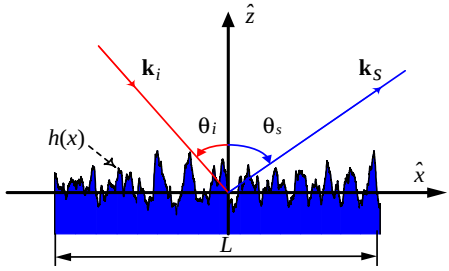

Figure 6. Geometry of the sea surface scattering problem.

horizontal and vertical components, respectively.

$$\begin{aligned} |\mathbf{k}_s| &= |\mathbf{k}_i| = k_i \\ \mathbf{k}_i &= k_{ix}\hat{\mathbf{x}} - q_{iz}\hat{\mathbf{z}} = k_i \sin\theta_i \hat{\mathbf{x}} - k_i \cos\theta_i \hat{\mathbf{z}}, \\ \mathbf{k}_s &= k_{sx}\hat{\mathbf{x}} + q_{sz}\hat{\mathbf{z}} = k_i \sin\theta_s \hat{\mathbf{x}} + k_i \cos\theta_s \hat{\mathbf{z}} \end{aligned} \tag{9}$$

The tapered incident field [32] can be expressed as

$$E_i(x) = G(x,h)\exp(-jk_i x) \tag{10}$$

$$G(x,h) = \exp\left\{-jk_i\left[x\sin\theta_i - h(x,t)\cos\theta_i\right]\frac{2\left[x+h(x,t)\tan\theta_i\right]^2/g_t^2 - 1}{\left(k_i g_t \cos\theta_i\right)^2}\right\} \times \exp\left\{-\frac{\left[x+h(x,t)\tan\theta_i\right]^2}{g_t^2}\right\} \tag{11}$$

g_t is the taper wave beam waist. Thus, the scattering amplitude for linear sea is expressed as

$$\begin{aligned} S(k_{sx},k_{ix};t) = &\frac{2\sqrt{q_{iz}q_{sz}}}{(q_{iz}+q_{sz})\sqrt{P}}\int\frac{dx}{(2\pi)}G(x,h) \\ &\exp\left[-j\left(k_{sx}-k_{ix}\right)x + j\left(q_{sz}+q_{iz}\right)h(x,t)\right] \\ &\times\left[B(k_{sx},k_{ix}) - \frac{j}{4}\int M(k_{sx},k_{ix};\zeta)H(\zeta,t)\exp(j\zeta x)\,\mathbf{d}\zeta\right] \end{aligned} \tag{12}$$

where $H(\zeta,t)$ is the Fourier transform of the surface elevation.

$$H(\zeta,t) = \frac{1}{(2\pi)}\int h(x,t)\exp(-j\zeta x)dx \tag{13}$$

P is the incident wave power captured by the sea surface. The details of kernel functions of the integral, B and M, can be found in [25], here, we safely omit it for the sake of brevity.

For revised CWM, the integral variables x in Equation (12) should be replaced by $\tilde{x} = x + C(x,t)$, thus the Jacobian J of the

transformation from x to $\tilde{x}$ is utilized to accomplish this change of integral variables. Equation (12) should be rewritten as

$$S(k_{sx}, k_{ix}; t) = \frac{2\sqrt{q_{iz}q_{sz}}}{(q_{iz}+q_{sz})\sqrt{P}} \int \frac{dx}{(2\pi)} \exp\left[-j\left(k_{sx}-k_{ix}\right)\left(x+C\left(x,t\right)\right)\right.$$
$$\left.+j\left(q_{sz}+q_{iz}\right)h\left(x,t\right)\right] \times G\left(x,h\right)J\left(x,t\right)$$
$$\left[B\left(k_{sx},k_{ix}\right)-\frac{j}{4}\int M\left(k_{sx},k_{ix};\zeta\right)H(\zeta,t)\exp(j\zeta x)\mathbf{d}\zeta\right] \quad (14)$$

where $J\left(x,t\right) = 1 + \partial C\left(x,t\right)/\partial x$.

The expression of the Doppler spectrum based on the periodogram method is given by

$$S_{\mathrm{Dop}}\left(f\right) = \left\langle \frac{1}{T}\left|\int_0^T S\left(k_{sx},k_{ix};t\right)\exp\left(-j2\pi ft\right)\mathrm{d}t\right|^2\right\rangle \quad (15)$$

where the angle bracket denotes the ensemble average over much surface realizations, and T is the duration of the sea surface evolution. In this paper, each Doppler spectrum is evaluated over 200 samples of the surface realizations involving time-varying sea surfaces with 256 time steps.

The Doppler shift f_s and bandwidth of the Doppler spectrum f_w are both the most important parameters of the Doppler spectrum, and their expressions are given respectively by

$$f_s = \frac{\int f S_{\mathrm{Dop}}\left(f\right)\mathrm{d}f}{\int S_{\mathrm{Dop}}\left(f\right)\mathrm{d}f}, \quad f_w^2 = \frac{\int \left(f-f_s\right)^2 S_{\mathrm{Dop}}\left(f\right)\mathrm{d}f}{\int S_{\mathrm{Dop}}\left(f\right)\mathrm{d}f} \quad (16)$$

4. NUMERICAL RESULTS

As aforementioned, the nonlinear hydrodynamics could well describe the wave-wave interactions, thus it is instructive to compare the Doppler spectra for the dynamic nonlinear choppy sea surfaces and that for the linear sea surfaces first. Unless otherwise noted, the wind speed u is 5 m/s, incident wave frequency 1.304 GHz, length of the simulated surface L 236 m, and taper wave beam wais chosen to be $L/6$ in the following calculations.

Figure 7 shows the normalized Doppler spectra of linear surfaces and the nonlinear choppy surfaces of infinite-depth seas. The corresponding Bragg frequencies are noted in the plots by the vertical black solid lines. First, at small incident angles, the Doppler spectra for linear sea surface and nonlinear choppy sea surface almost coincide with each other, because at small incident angles, the influence of the

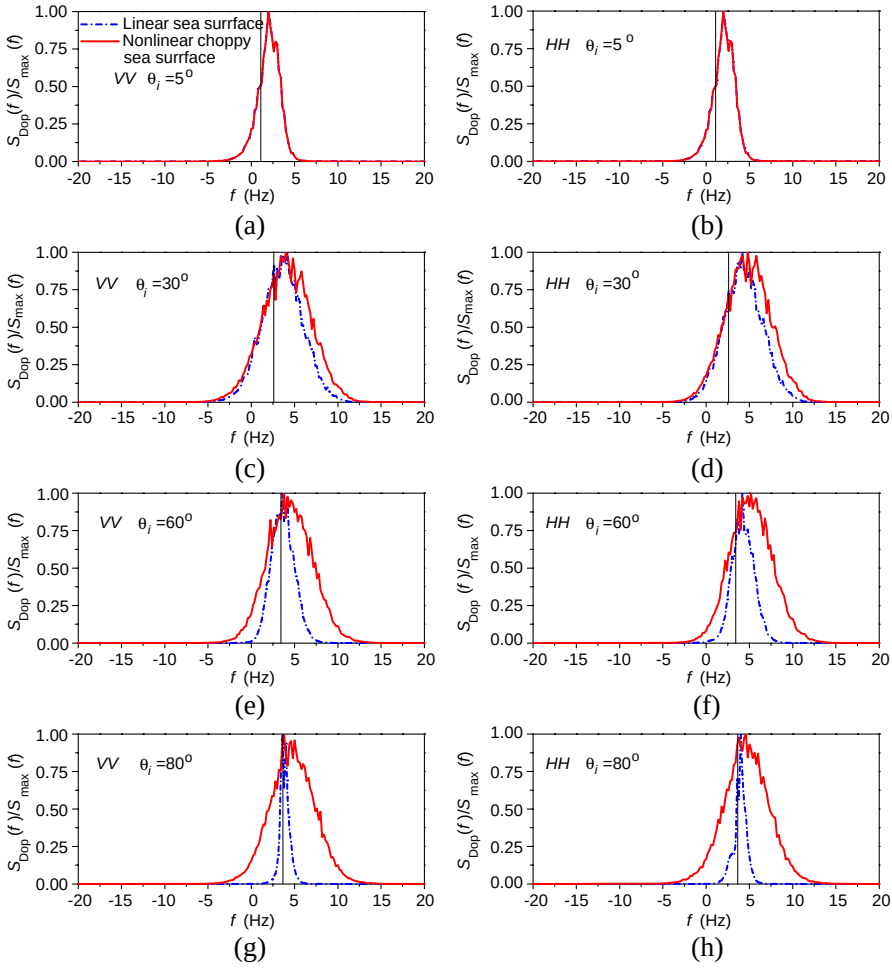

Figure 7. The normalized Doppler spectra of linear surfaces and the nonlinear choppy surfaces of infinite-depth seas. The wind speed u is 5 m/s.

horizontal velocity component on the Doppler spectrum is also small. When the incident angle increases, the Doppler spectra for nonlinear sea surface are much wider than their counterpart of the linear sea surface, because the nonlinear-wave components propagate faster than the linear-wave components. Second, as incident angle increases, for nonlinear sea surface, the Doppler peak frequency is continuously away from the Bragg frequency as incident angle increases, even in the case of near grazing incidence, because CWM corrects the horizontal

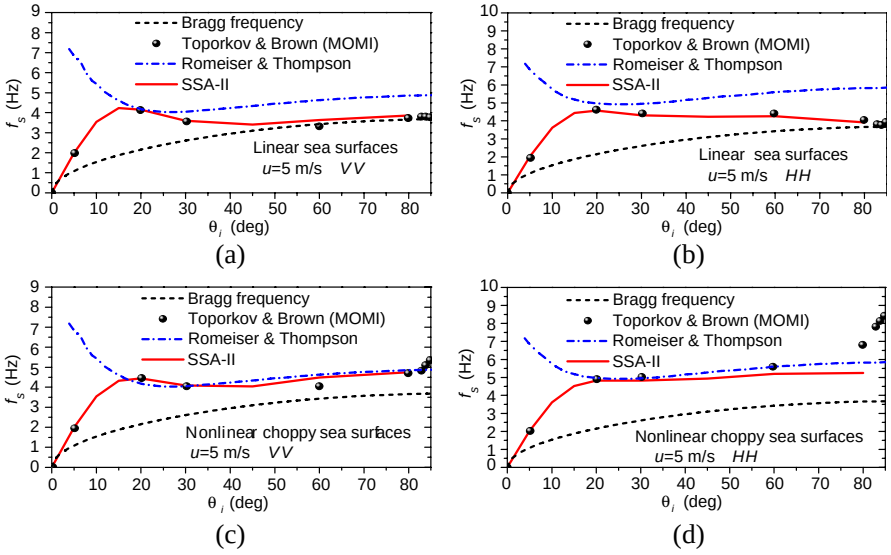

Figure 8. Variation of Doppler shifts with incident angles for linear surfaces and the nonlinear choppy surfaces of infinite-depth seas.

component of particle velocities by adding a displacement related to the surface elevation to the horizontal position of the particles, which remarkably affect the Doppler spectrum. These conclusions are also supported by those found in [28].

In Figure 8 and Figure 9, the Doppler shifts and bandwidths of the Doppler spectra presented in Figure 7 are evaluated. Two data sets as references are quoted here. One is the data set of Doppler simulations based on rigorous MOMI model by Toporkov and Brown [15], and the other is based on the TSM combined with the modulation transfer function (MTF) technique by Romeiser and Thompson [33], which has been demonstrated to be qualitatively consistent with the experimental results and other numerical approaches.

From Figure 8, it is evident that the Doppler shift predicted by SSA-II and the MOMI agrees excellently for vertical polarization (VV), and the agreement for horizontal polarization (HH) is also pretty good except at grazing incident angles for nonlinear choppy surfaces. At $\theta_i = 80°$, both the analytic model results of Romeiser and Thompson's TSM combing MTF, and SSA-II are less than the MOMI data of an explosively high value. It is indicated that the problem for grazing incidence known in the evaluation of radar cross section (RCS) is still a tough issue for Doppler spectrum simulation under certain circumstance.

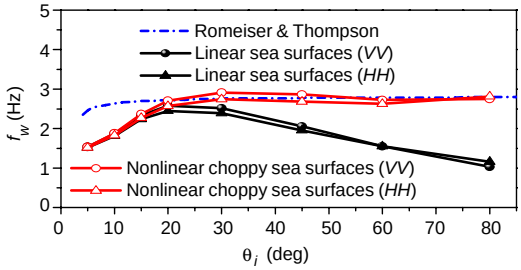

Figure 9. Variation of spectra bandwidths with incident angles for linear surfaces and the nonlinear choppy surfaces of infinite-depth seas.

In Figure 9, as the incident angle increases, the bandwidth of the Doppler spectrum for linear surface first increases and then decreases rapidly, while for nonlinear sea surface, the bandwidth first increases as the linear surface does, and then maintains at a relatively stable value at larger incident angles ($> 30°$), which agrees better with Romeiser and Thompson model data. From Figure 8 and Figure 9, it can be concluded that the SSA-II model is very reliable for the Doppler spectrum simulation, even for the nonlinear sea surface containing steeper crests with larger slope, which prompts us to investigate the Doppler spectra of backscattered echoes from nonlinear finite-depth sea based on aforementioned evaluations.

In Figure 10, we show the Doppler spectra of backscattered echoes from nonlinear sea for different water depths. The wind speed is 10 m/s, and water depths are chosen as infinite, 8 m, 4 m and 2 m respectively. Other simulation parameters are the same as those in Figure 8. It is shown that at $\theta_i = 5°$, the peak frequency is slightly smaller for both polarizations when the water depth decreases; as incident angle increases to 30°, however, the peak frequency for shallower sea shifts toward a much higher value, because at small incident angles (5°), based on the stationary phase theory in EM scattering, the scattered fields are mainly contributed by large-scale long waves. However, when the water depth decreases, the long waves are gradually suppressed, and shorter wind waves become more and more. Thus the Doppler spectrum features determined by the velocities of the specular scattering particles are also suppressed. As the incident angle increases, the main contribution to scatterer fields will come from the diffuse scattering dominated by small-scale short waves, thus the Doppler shift and bandwidth of the Doppler spectrum for shallower sea (2 m) will gradually overwhelm their counterpart of the deeper sea.

The Doppler shifts and bandwidths of the Doppler spectra in Figure 10 are further investigated in Figure 11. As shown in

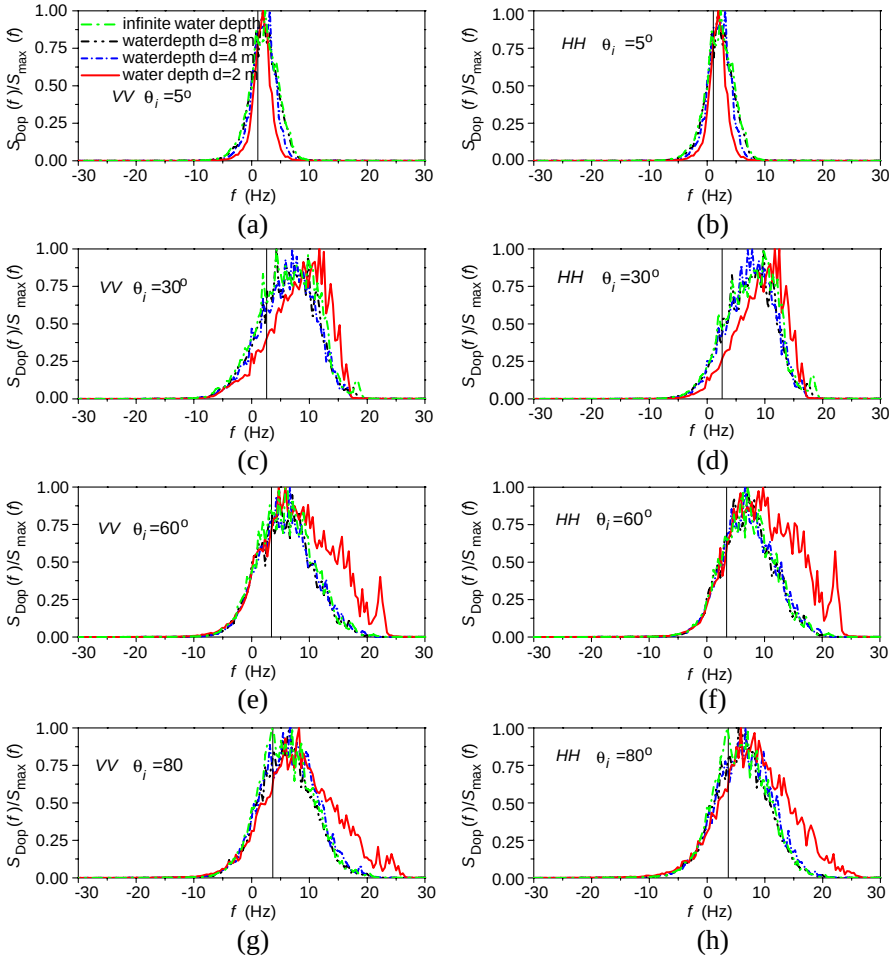

Figure 10. Doppler spectra of backscattered echoes from nonlinear sea for different water depths. The wind speed is 10 m/s.

Figures 11(a) and (b), the Doppler shift for surfaces of a sea with fixed depth almost does not show any polarization difference below the incident angle of 15°. As the incident angle increases, the Doppler shifts corresponding to different polarizations become separated: the HH-polarized Doppler shift is much larger than its counterpart of the VV polarization. This phenomenon is similar with the situation presented in Figures 8(c) and (d). It is implied that the finite-depth sea surface in this study is one of the special cases of nonlinear surface with much more intense nonlinear hydrodynamic effect. From Figures 11(c)

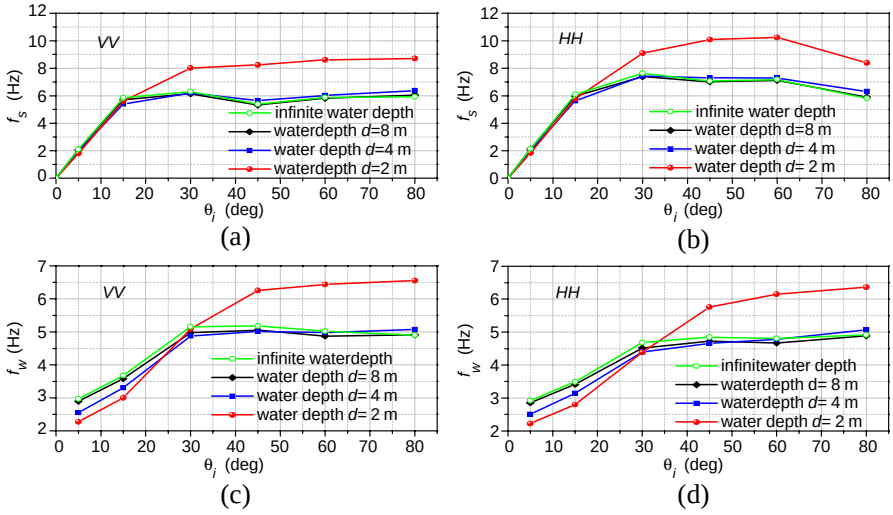

Figure 11. (a) (b) The Doppler shifts and (c) (d) bandwidths of the Doppler spectra for sea surfaces with different depths. The wind speed is 10 m/s.

and (d), it can be found that at small incident angles, the spectrum bandwidth for the shallowest sea (2 m depth) corresponds to the smallest value among the three curves. When the incident angle rises, the opposite situation can be gradually observed. This phenomenon may reflect the fact that the shallower water can sustain only shorter wind waves, which mainly contributes to the diffuse scattering field of the dynamic sea surface at intermediate to large incident angles.

5. CONCLUSION

In this paper, Doppler spectral characteristics of electromagnetic backscattered echoes from dynamic nonlinear surfaces of finite-depth sea have been investigated using SSA-II combining the revised CWM. The investigation of Doppler spectral characteristics of backscattered echoes from linear surfaces and nonlinear choppy sea surfaces are conducted first. It can be found that the Doppler spectra are significantly affected by the nonlinear hydrodynamic effects among sea waves, which should be given adequate consideration in the Doppler spectra analysis. The comparison between predicted Doppler spectral parameters and the rigorous numerical model results shows good agreement, which verifies the model in this paper. When both are

based on the nonlinear CWM, the Doppler spectra of backscattered echoes from finite-depth sea with different depths are evaluated. The numerical results show that the nonlinear interactions among waves in shallower sea are much more intense. Moreover, at small incident angles, the Doppler shifts and spectra bandwidths are much lower for shallower sea, and the opposite situation can be gradually observed for increased incident angles. It is indicated that the long waves are gradually suppressed while the shorter wind waves are boosted as water depth decreases, which weakens the specular scattering field and enhances the diffuse scattering one. Thus corresponding velocities of the scattering particles are also affected. Although the work is limited to the 1-D surface, the analysis presented and conclusions obtained in this paper will help to better investigate the Doppler spectral characteristics of backscattered signals from the dynamic surfaces of finite-depth nearshore seas.

ACKNOWLEDGMENT

The authors would like to thank the Fundamental Research Funds for the Central Universities, the National Natural Science Foundation of China under Grant No. 60871070, and the Foundation of the Science and Technology on Electromagnetic Scattering Laboratory to support this kind of research.

REFERENCES

1. Kurrant, D. J. and E. C. Fear, "Extraction of internal spatial features of inhomogeneous dielectric objects using near-field reflection data," *Progress In Electromagnetics Research*, Vol. 122, 197–221, 2012.
2. Chen, H., M. Zhang, and H.-C. Yin, "Facet-based treatment on microwave bistatic scattering of three-dimensional sea surface with electrically large ship," *Progress In Electromagnetics Research*, Vol. 123, 385–405, 2012.
3. Yang, W., Z.-Q. Zhao, C.-H. Qi, W. Liu, and Z.-P. Nie, "Iterative hybrid method for electromagnetic scattering from a 3-D object above a 2-D random dielectric rough surface," *Progress In Electromagnetics Research*, Vol. 117, 435–448, 2011.
4. Baussard, A., M. Rochdi, and A. Khenchaf, "PO/Mec-based scattering model for complex objects on a sea surface," *Progress In Electromagnetics Research*, Vol. 111, 229–251, 2011.

5. Ji, W.-J. and C.-M. Tong, "Bistatic scattering from two-dimensional dielectric ocean rough surface with a PEC object partially embedded by using the G-SMCG method," *Progress In Electromagnetics Research*, Vol. 105, 119–139, 2010.
6. Luo, W., M. Zhang, Y.-W. Zhao, and H. Chen, "An efficient hybrid high-frequency solution for the composite scattering of the ship on very large two-dimensional sea surface," *Progress In Electromagnetics Research M*, Vol. 8, 79–89, 2009.
7. Fabbro, V., "Apparent radar cross section of a large target illuminated by a surface wave above the sea," *Progress In Electromagnetics Research*, Vol. 50, 41–60, 2005.
8. Zhang, M., Y.-W. Zhao, H. Chen, and W.-Q. Jiang, "SAR imaging simulation for composite model of ship on dynamic ocean scene," *Progress In Electromagnetics Research*, Vol. 113, 395–412, 2011.
9. Chen, H., M. Zhang, D. Nie, and H. C. Yin, "Robust semi-deterministic facet model for fast estimation on EM scattering from ocean-like surface," *Progress In Electromagnetics Research B*, Vol. 18, 347–363, 2009.
10. Nie, D. and M. Zhang, "Bistatic scattering analysis for two-dimensional rough sea surfaces using an angular composite model," *Int. J. Remote Sens.*, Vol. 32, No. 24, 9661–9672, 2011.
11. Mouche, A. A., B. Chapron, N. Reul, and F. Collard, "Predicted Doppler shifts induced by ocean surface wave displacements using asymptotic electromagnetic wave scattering theories," *Waves Random Complex Media*, Vol. 18, No. 1, 185–196, 2008.
12. Zavorotny, V. U. and A. G. Voronovich, "Two-scale model and ocean radar Doppler spectra at moderate- and low-grazing angles," *IEEE Trans. Antennas Propag.*, Vol. 46, No. 1, 84–92, 1998.
13. Rino, C. L., T. L. Crystal, A. K. Koide, H. D. Ngo, and H. Guthart, "Numerical simulation of backscattering from linear and nonlinear ocean surface realizations," *Radio Sci.*, Vol. 26, No. 1, 51–71, 1991.
14. Creamer, D. B., F. Henyey, R. Schult, and J. Wright, "Improved linear representation of sea surface waves," *J. Fluid Mech.*, Vol. 205, 135–161, 1989.
15. Toporkov, J. V. and G. S. Brown, "Numerical simulations of scattering from time-varying, randomly rough surfaces," *IEEE Trans. Geosci. Remote Sens.*, Vol. 38, No. 4, 1616–1625, 2000.
16. Johnson, J. T., J. V. Toporkov, and G. S. Brown, "A numerical study of backscattering from time-evolving sea surfaces:

Comparison of hydrodynamic models," *IEEE Trans. Geosci. Remote Sens.*, Vol. 39, No. 11, 2411–2420, 2001.

17. Soriano, G., M. Joelson, and M. Saillard, "Doppler spectra from a two-dimensional ocean surface at L-band," *IEEE Trans. Geosci. Remote Sens.*, Vol. 44, No. 9, 2430–2437, 2006.
18. Nouguier, F., C. A. Guérin, and G. Soriano, "Analytical techniques for the Doppler signature of sea surfaces in the microwave regime II: Nonlinear surfaces," *IEEE Trans. Geosci. Remote Sens.*, Vol. 49, No. 12, 4920–4927, 2011.
19. Nouguier, F., C. A. Guérin, and B. Chapron, "Choppy wave model for nonlinear gravity waves," *J. Geophys. Res. (JGR) — Oceans*, Vol. 114, No. C09012, 1–16, 2009.
20. Barrick, D. E. and B. J. Lipa, "The second-order shallow-water hydrodynamic coupling coefficient in interpretation of HF radar sea echo," *IEEE J. Ocean. Eng.*, Vol. 11, No. 2, 310–315, 1986.
21. Lipa, B. J. and D. E. Barrick, "Extraction of sea state from HF radar sea echo: Mathematical theory and modeling," *Radio Sci.*, Vol. 21, No. 1, 81–100, 1986.
22. Holden, G. J. and L. R. Wyatt, "Extraction of sea state in shallow water using HF radar," *Proc. Inst. Elect. Eng. F — Radar Signal Process.*, Vol. 139, No. 2, 175–181, 1992.
23. Qi, C., Z. Zhao, W. Yang, Z.-P. Nie, and G. Chen, "Electromagnetic scattering and Doppler analysis of three-dimensional breaking wave crests at low-grazing angles," *Progress In Electromagnetics Research*, Vol. 119, 239–252, 2011.
24. Luo, W., M. Zhang, C. Wang, and H.-C. Yin, "Investigation of low-grazing-angle microwave backscattering from three-dimensional breaking sea waves," *Progress In Electromagnetics Research*, Vol. 119, 279–298, 2011.
25. Voronovich, A. G. and V. U. Zavorotny, "Theoretical model for scattering of radar signals in Ku- and C-bands from a rough sea surface with breaking waves," *Waves Random Media*, Vol. 11, No. 3, 247–269, 2001.
26. Soriano, G. and M. Saillard, "Modelization of the scattering of electromagnetic waves from the ocean surface," *Progress In Electromagnetics Research*, Vol. 37, 101–128, 2002.
27. Berginc, G., "Small slope approximation method: A further study of vector wave scattering from two-dimensional surfaces and comparison with experimental data," *Progress In Electromagnetics Research*, Vol. 37, 251–287, 2002.
28. Li, X.-F. and X.-J. Xu, "Scattering and Doppler spectral analysis

for two-dimensional linear and nonlinear sea surfaces," *IEEE Trans. Geosci. Remote Sens.*, Vol. 49, No. 2, 603–611, 2011.

29. McCormick, M. E., *Ocean Engineering Wave Mechanics*, John Wiley & Sons Inc, New York, 1973.
30. Hasselmann, K., et al., "Measurements of wind-wave growth and swell decay during the Joint North Sea Wave Project (JONSWAP)," *Dtsch. Hydrogr. Z. Suppl.*, Vol. 12, No. A8, 1–95, 1973.
31. Miche, M., "Mouvements ondulatoires de la mer en profondeur constante ou décroissante. forme limite de la houle lors de son d'eferlement. Application aux digues marines," *Ann. Ponts Chaussées*, Vol. 114, 25–78, 1944.
32. Tsang, L., J. A. Kong, and K. H. Ding, *Scattering of Electromagnetic Waves,* John Wiley & Sons Inc., New York, 2001.
33. Romeiser, R. and D. R. Thompson, "Numerical study on the along-track interferometric radar imaging mechanism of oceanic surface currents," *IEEE Trans. Geosci. Remote Sens.*, Vol. 38, No. 1, 446–458, 2000.